

RESEARCH

Open Access



# Tensile Behavior of High-Strength Stainless Steel Wire Rope (HSSSWR)-Reinforced ECC

Xinling Wang<sup>1</sup>, Guanghua Yang<sup>1</sup>, Wenwen Qian<sup>2</sup>, Ke Li<sup>1\*</sup> and Juntao Zhu<sup>1</sup>

## Abstract

Engineered cementitious composites (ECC) show the distinguished characteristics of high post-cracking resistance and ductility. High-strength stainless steel wire rope (HSSSWR) has been successfully used for restoring or strengthening of existing structures. By combining the advantages of these two materials, a new composite system formed by embedding HSSSWR into ECC was proposed and expected to be a promising engineering material for repair or strengthening of structures. To investigate the tensile failure mechanism and mechanical properties of HSSSWR-reinforced ECC, an experimental study on 27 HSSSWR-reinforced ECC plates was conducted considering the effects of the reinforcement ratio of longitudinal HSSSWRs, formula of ECC and width of the plate. Test results revealed that HSSSWR-reinforced ECC exhibit superior post-cracking resistance, deformation capacity and crack-width control capacity. Increasing the reinforcement ratio of longitudinal HSSSWRs can effectively enhance the tensile strength, crack-width control capacity, deformation capacity and tensile toughness of HSSSWR-reinforced ECC. Adding thickener in ECC can significantly improve the crack-width control capacity and deformation capacity of HSSSWR-reinforced ECC due to enhancing uniform distribution of polyvinyl alcohol fibers, but would slightly reduce the cracking stress and maximum tensile stress by bringing small bubbles in the matrix. The tensile properties of HSSSWR-reinforced ECC plates are almost not affected by varying the plate width. Besides, a tensile constitutive model was developed for charactering the stress–strain relationship of HSSSWR-reinforced ECC in tension. Based on mechanical theories and failure characteristics of HSSSWR-reinforced ECC, the model parameters were determined, and calculation equations of cracking stress and tensile strength were proposed. The accuracy of the developed model and calculation equations was verified by test results.

**Keywords:** engineered cementitious composites (ECC), high-strength stainless steel wire rope (HSSSWR), mechanical properties, tensile constitutive model

## 1 Introduction

Engineered cementitious composites (ECC) are developed by using performance driven design approach of short random fibers reinforced cementitious matrix composites, which have distinguished material properties such as remarkably high post-cracking resistance, tensile ductility and toughness (Li, 2019; Li & Leung, 1992; Li et al., 1993, 1995, 2004; Zhou et al., 2015). Compared

with traditional fiber-reinforced concrete, ECC show the more excellent characteristics of pseudo-strain-hardening behavior and multiple cracking in tension (Li et al., 1995; Naaman & Reinhardt, 2006), and have been successfully applied to civil engineering (Esmaeeli et al., 2013; Fischer & Li, 2002a; Guan et al., 2018; Hung & Chen, 2016; Pan et al., 2020; Qi et al., 2018; Shang et al., 2019; Yuan et al., 2014; Zheng et al., 2016). Many scholars have carried out a lot of investigations on existing members strengthened with ECC (Esmaeeli et al., 2013; Hung & Chen, 2016; Shang et al., 2019; Zheng et al., 2016), which demonstrated that ECC can significantly increase the deformation capacity, energy absorption capacity and

\*Correspondence: irwinlike@163.com

<sup>1</sup> School of Civil Engineering, Zhengzhou University, Science Avenue 100#, Zhengzhou 450001, China

Full list of author information is available at the end of the article

Journal information: ISSN 1976-0485 / eISSN 2234-1315

crack control capacity when used to strengthen existing masonry or reinforced concrete (RC) structures. However, the strengthening effect of ECC on bearing capacity of existing structural members is limited due to the limited tensile strength of ECC. Therefore, ECC still need to be used together with other high-strength reinforcing materials. Many researches have been conducted on ECC reinforced with steel reinforcements (Fischer & Li, 2002b; Kunieda et al., 2010) and fiber-reinforced polymer (FRP) reinforcements (Al-Gemeel et al., 2019; Hossain, 2018; Hu et al., 2019; Li & Xiong, 2019; Zheng et al., 2016; Zhu et al., 2018).

Fischer and Li (Fischer & Li, 2002b) performed uniaxial tensile tests to investigate the influence of composite ductility on the deformation behavior of the steel reinforced ECC and its effects on the strain distribution in the reinforcement, composite matrix, and interfacial bond. The results revealed the good deformation combination of ECC and steel reinforcement which led to a more uniform strain distribution in reinforcement and ECC and controlled damage at relatively large inelastic deformations. Kunieda et al. (Kunieda et al., 2010) assessed the effect of different steel reinforcement ratios on crack distribution of ultrahigh performance-strain hardening cementitious composites (UHP-SHCC) through the tensile tests. It was found that the increase of steel reinforcement ratio could lead to the increase of the number of cracks and the decrease of the averaged crack spacing, and the influence was insignificant when the reinforcement ratio was beyond 0.6%. Zhu et al. (Zhu et al., 2018) conducted an experiment study on the uniaxial tensile behavior of carbon fiber-reinforced polymer (CFRP) grid-reinforced ECC plates under both monotonic and cyclic loading. Test results indicate that the envelope of cyclic uniaxial tensile stress–strain curves followed the static stress–strain curves no matter which cyclic loading scheme was adopted. Al-Gemeel et al. (Al-Gemeel et al., 2019) investigated the tensile performance of ring-shape specimens reinforced with basalt fiber-reinforced polymer (BFRP) grids and ECC under apparent hoop tensile loading, and found that compared with ECC without BFRP grids and conventional mortar reinforced by BFRP grids, the first crack load, peak load and energy absorption ability of BFRP grid-reinforced ECC were improved more notably. Although existing studies (Al-Gemeel et al., 2019; Fischer & Li, 2002b; Hossain, 2018; Hu et al., 2019; Kunieda et al., 2010; Li & Xiong, 2019; Zheng et al., 2016; Zhu et al., 2018) show that ECC reinforced by steel or FRP reinforcements were feasible reinforcement materials for strengthening or rehabilitation of concrete structures and can effectively improve ductility, anti-cracking ability and bearing capacity of RC structures, some deficiencies of these strengthening materials

remained. Specifically, the ultrahigh deformation capacity of ECC cannot be fully utilized on account of the low tensile strength and early yielding of ordinary steel bars, when using ordinary steel bars to reinforce ECC. In addition, although FRP features the light weight, high tensile strength and good corrosion resistance, the rupture strains of FRP grids were much lower than the ultimate strain of ECC, which would cause the underutilization of ultrahigh deformation capacity of ECC. Moreover, FRP costs relatively more than other conventional reinforcing materials, which would be an impediment to their promotion and application in the common constructions. Therefore, a more appropriate reinforcing material with relatively high strength, low price and ultimate strain close to the ultimate strain of ECC needs to be used for reinforce ECC to provide better reinforcement effect.

High-strength stainless steel wire rope (HSSSWR) features relatively high tensile strength, good anti-corrosion performance and relatively low price (Kim & Kim, 2011). Steel wire ropes or steel wires in combination with epoxy resins, plain mortar or permeable polymer mortar have been successfully applied to restore or increase the capacity of existing masonry or concrete structures (Ghai et al., 2018; Kim & Kim, 2011; Li et al., 2018; Qeshta et al., 2015; Shermi & Dubey, 2017). Nevertheless, previous studies (Ghai et al., 2018; Huang et al., 2011; Kim & Kim, 2011; Shermi & Dubey, 2017) show that the ultimate strength of the steel wire ropes or steel wires cannot be effectively exerted due to the brittle fracture of mortar or permeable polymer mortar before the failure of steel wire ropes or steel wires. Moreover, the disadvantages of epoxy resins have been progressively observed by researchers, including high cost, poor performance on wet surfaces or after ultraviolet radiation, and poor fire resistance, etc. (Qeshta et al., 2016; Raoof et al., 2017). Therefore, HSSSWR needs to be used with a matrix material of good crack-control capacity and ductility to give full play to high strength of HSSSWR.

As discussed above, compared with mortar and permeable polymer mortar, ECC exhibit much more excellent ductility and crack-control capacity. Besides, the ultimate tensile strain of HSSSWR, which is characterized by high tensile strength, good anti-corrosion performance and relatively low price, is about 3%, and is close to the ultimate tensile strain of ECC. Furthermore, good bond performance between HSSSWR and ECC has been revealed by Zhu et al. (Wang et al., 2020; Zhu et al., 2020). Therefore, HSSSWR could be appropriate reinforcing materials for ECC to give full play to the excellent performance of ECC, and ECC would be suitable matrix for HSSSWR to fully exert the high tensile strength of HSSSWR. Combining the advantages of both HSSSWR and ECC, a new composite system, namely HSSSWR-reinforced ECC,

which is formed by embedding HSSSWR into ECC, was proposed, and the flexural strengthening method with HSSSWR-reinforced ECC was verified to result in a more significant increase in deformation capacity, crack-width control capacity, stiffness, cracking strengths and ultimate strengths of RC beams, compared with strengthening method by using HSSSWR and polymer mortar (Yuan et al., 2020). Accordingly, HSSSWR-reinforced ECC is expected to be a promising engineering material for repair or strengthening of structures.

In order to promote the applications of HSSSWR-reinforced ECC in strengthening of existing structures which would often make this new composite material subjected to tension, it is of great need to comprehensively understand the tensile properties of HSSSWR-reinforced ECC. Furthermore, it is essential to develop a tensile constitutive model of HSSSWR-reinforced ECC which would be needed for finite element analysis of the mechanical behavior of existing structures strengthened by HSSSWR-reinforced ECC, when HSSSWR-reinforced ECC are considered to be a kind of composite material to simplify the calculation. Therefore, in this paper, a total of 27 specimens were designed to investigate the tensile behavior of HSSSWR-reinforced ECC plates, considering the effects of reinforcement ratio of longitudinal HSSSWRs, formula of ECC and width of the test specimen. The experimental study aims to (1) evaluate the influences of the parameters mentioned above on the tensile behavior of HSSSWR-reinforced ECC; (2) determine the prediction formulas for cracking stress and tensile strength of this composite material, and (3) develop a tensile constitutive model of this composite material and validate the accuracy of this model using the test results.

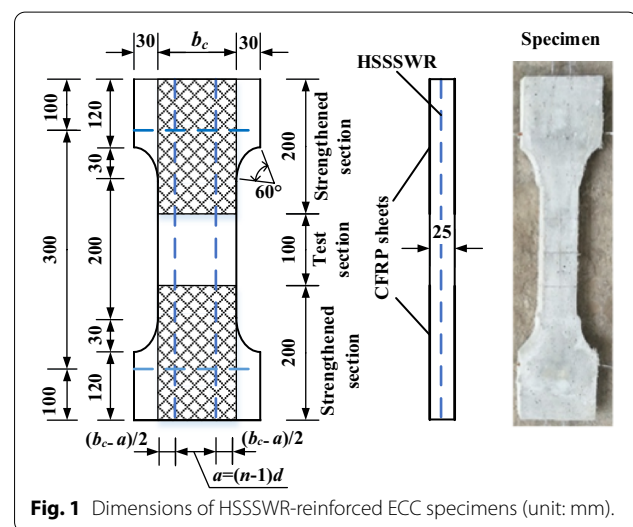
## 2 Experimental Program

### 2.1 Design of Specimens

In this study, a total of 27 specimens were designed to evaluate the effects of variables on tensile behavior of HSSSWR-reinforced ECC by using uniaxial tensile tests. The test variables included the reinforcement ratio of HSSSWR, formula of ECC and width of HSSSWR-reinforced ECC specimens. The design details of all test specimens are summarized in Table 1. In Table 1,  $b_c$  is the test section width of HSSSWR-reinforced ECC specimens,  $n$  is the number of longitudinal HSSSWRs used in the specimen, and  $d$  and  $\rho_w$  represent the spacing and reinforcement ratio of longitudinal HSSSWRs. In the test, there were totally 9 groups of specimens with 3 identical specimens for each group. The tensile plate specimens are designed in the shape of dumbbell. In order to avoid failure caused by stress concentration in the specimen beneath the clamp during the loading process, two ends of each specimen were strengthened by CFRP sheets.

**Table 1** Parameters of HSSSWR-reinforced ECC specimens.

Group	Group number	$b_c$ (mm)	$n$	$d$ (mm)	$\rho_w$
A	A1	80	2	50	0.0028
	A2	70	2	40	0.0032
	A3	60	2	30	0.0037
	A4	50	2	20	0.0048
	A5	90	3	30	0.0037
B	B1	80	2	50	0.0028
	B2	70	2	40	0.0032
	B3	60	2	30	0.0037
	B4	50	2	20	0.0048



The CFRP sheets were bonded to the both surfaces symmetrically of the specimens by epoxy resin. Furthermore, the curved sides of the specimen were applied to ensure a smooth transition to avoid stress concentration. Fig. 1 shows the detailed dimensions of the specimens.

### 2.2 Material Properties

ECC were manufactured using ordinary Portland cement (PO 42.5), fly ash, silica fume, silica sand, polyvinyl alcohol (PVA) fibers, water, superplasticizer and thickener. The two mix proportions of the specimens in this paper are given in Table 2. When casting the HSSSWR-reinforced ECC plate specimens, three ECC cubes of 70.7-mm side length and five ECC thin plates (with dimensions of 280 mm × 40 mm × 15 mm) are manufactured for uniaxial compression and tension tests, respectively, to determine the material properties of each kind of ECC used in the test. Table 3 lists the average values of key parameters for ECC material properties including initial crack stress in tension ( $f_{e,cr}$ ) and its corresponding

strain ( $\epsilon_{e,cr}$ ), the ultimate tensile stress ( $f_{e,u}$ ) and its ultimate tensile strain ( $\epsilon_{e,u}$ ), the compressive strength ( $f_c$ ) and its corresponding strain ( $\epsilon_c$ ), and elastic modulus ( $E_e$ ). Fig. 2 shows the tension test setup and the test results (including typical tensile stress–strain curves and crack patterns) of ECC, which indicated the characteristics

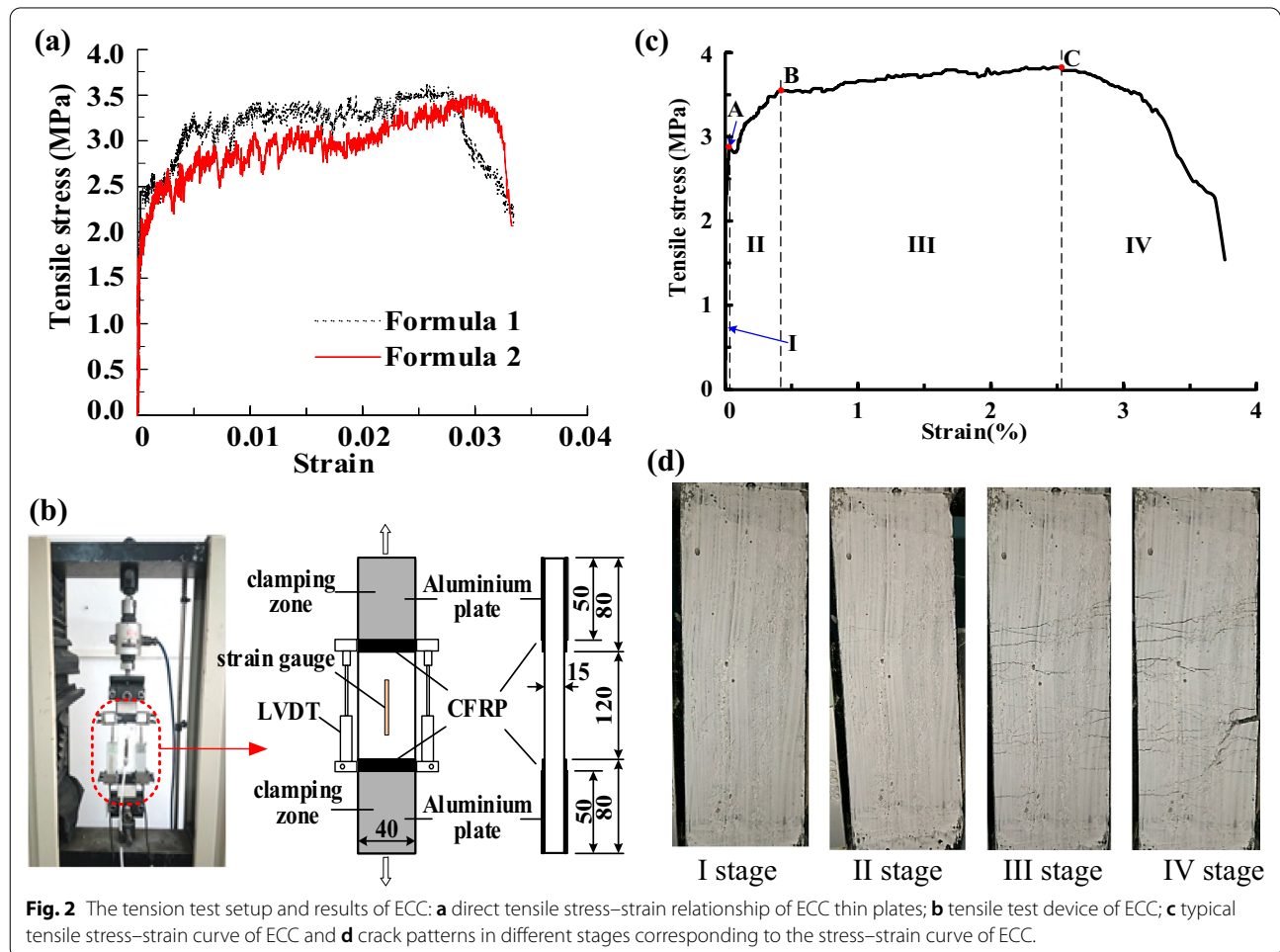
of pseudo strain-hardening and multiple cracking for ECC. The ECC of formula 2 exhibited higher deformation capacity and lower tensile strength, compared with the ECC of formula 1. In addition, tensile tests were performed on three HSSSWR specimens to determine the mechanical properties of the used HSSSWR with a

**Table 2** Mix proportions of ECC.

Types	Cement	Sand	Fly ash	Silica fume	Water	PVA fiber	Superplasticizer	Thickener
Formula 1	1	0.3	4	0.08	1	2%	0.06	0
Formula 2	1	0.3	4	0.08	1	2%	0.06	0.006

**Table 3** Test results of ECC material properties.

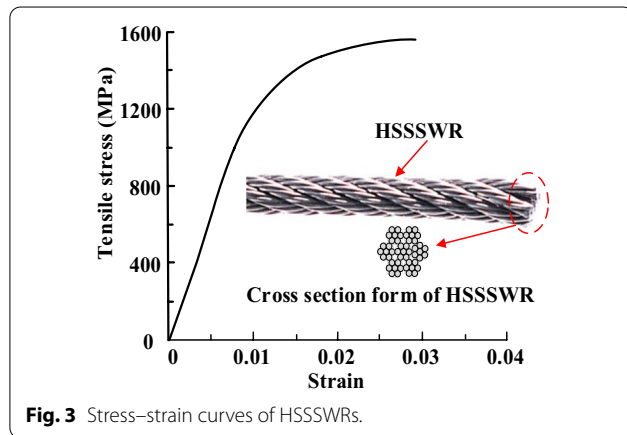
Types	$f_{e,cr}$ (N/mm <sup>2</sup> )	$\epsilon_{e,cr}$	$f_{e,u}$ (N/mm <sup>2</sup> )	$\epsilon_{e,u}$	$f_c$ (N/mm <sup>2</sup> )	$\epsilon_c$	$E_e$ (MPa)
Formula 1	2.19	0.0190%	3.53	2.79%	44.65	0.43%	11,500
Formula 2	1.92	0.0171%	3.46	2.97%	36.05	0.43%	11,250



diameter of 2.4 mm. The tested average elastic modulus ( $E_s$ ), ultimate tensile strength ( $f_y$ ) and its corresponding the tensile strain ( $\epsilon_u$ ) of the HSSWR were 108.3 GPa, 1567 MPa and 0.0303, respectively. The tested typical stress–strain curve and cross-sectional form of HSSWR are shown in Fig. 3.

### 2.3 Test Setup and Instrumentation

To research the tensile behavior of HSSWR-reinforced ECC plates, a series of uniaxial tension tests were conducted by using a 100-kN capacity electronic universal testing machine (Fig. 4). All tests were carried out under displacement control at the rate of 0.2 mm/min. For each specimen, two strain gauges were attached at the middle of the front and back surfaces of the specimen and two LVDTs were installed on both sides of the specimen. Load was measured by a load cell with a range of 100 kN.

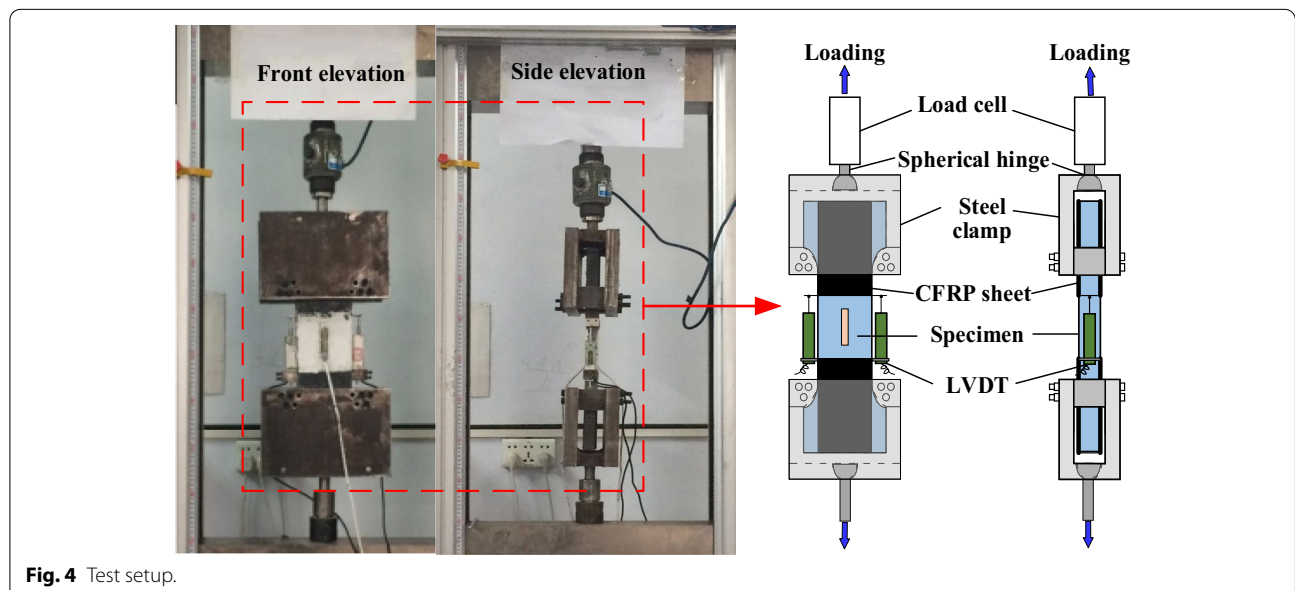
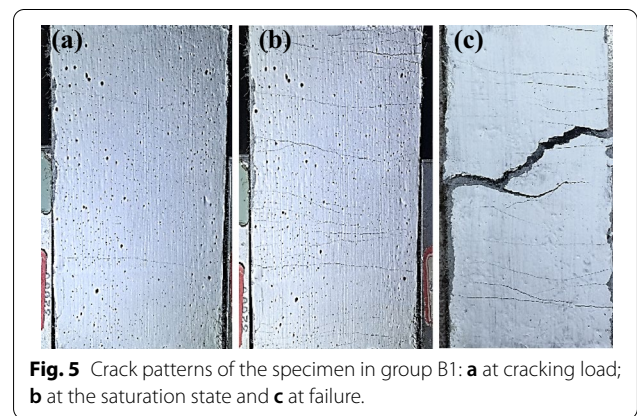


In addition, the crack-width of the specimens was measured by a crack detector instrument.

## 3 Experimental Results and Discussion

### 3.1 Test Phenomenon and Results

The tensile failure process of HSSWR-reinforced ECC specimens is shown in Fig. 5. When the applied load reached a certain value (23%–31% of the peak load), a tiny crack with a width of only 0.02 mm appeared on the surface near the middle of the specimens (Fig. 5(a)). As the load continued to increase, new cracks appeared continuously on the surface of the specimens, but the width of the existing cracks increased slowly. After reaching a certain load (84%–96% of the peak load), the number of cracks stopped increasing, which is referred to as the



saturation state, as shown in Fig. 5(b), and the surfaces of the specimens were covered with fine cracks almost parallel to each other. At this time, the maximum crack widths of the specimens were between 0.08 mm and 0.28 mm, which are much less than the crack-width limits in the normal service limit state of 0.3 mm and 0.4 mm required by Chinese design specification of concrete structures (Ministry of Housing and Urban–Rural Development of the People’s Republic of China (MOHURD): Code for Design of Concrete Structures 2015) and ACI 224 (Committee, 2001), respectively. Then as the load increased, the widths of existing cracks grew steadily. When the peak load was reached, a few small cracks connected to form a main crack on the monitored zone of the specimen, accompanied by clear sounds of pulling out or fracture of PVA fibers, and one longitudinal HSSWR ruptured at the main crack. Then the load fell rapidly, and the other longitudinal HSSWRs ruptured as the width of the main crack quickly increased, after which the test was stopped. It can be observed that the HSSWRs in the specimen did not rupture at the same time in the test. This may be because of the small differences between tensile stresses of longitudinal HSSWRs in the specimen under axial tension due to the different tightness of HSSWRs which may occur during manufacturing specimens. The maximum crack widths of the specimens at peak load were in the range of 0.5 mm–1.13 mm. The typical failure mode of the specimens is shown in Fig. 5(c). Those phenomena indicate that HSSWR-reinforced ECC have good post-cracking resistance and crack-width control capacity due to multiple cracking characteristic of ECC and good bond property of the HSSWR and ECC.

Table 4 shows average values of test results of cracking stress ( $f_{se,cr}$ ), cracking strain ( $\epsilon_{se,cr}$ ), maximum tensile stress ( $f_{se,u}$ ), the strain corresponding to  $f_{se,u}$  ( $\epsilon_{se,u}$ ), the tensile stress at the beginning of the saturation state ( $f_{ws}$ ), the strain corresponding to  $f_{ws}$  ( $\epsilon_{ws}$ ), the maximum crack-width at the beginning of the saturation state ( $w_{max,ws}$ ), the

maximum crack-width at peak load ( $w_{max,u}$ ), the elastic modulus before cracking ( $E_{se}$ ), the peak tensile toughness index ( $TI_p$ ) and the total tensile toughness index ( $TI_t$ ) for each group of specimens.

### 3.2 Stress–Strain Curves

Fig. 6 describes the tensile stress–strain curves of ECC and HSSWR-reinforced ECC specimens. As shown in Fig. 6, three main stages can be obviously observed in the tensile stress–strain curves of ECC and HSSWR-reinforced ECC specimens, as follows: (1) linear elastic stage; (2) elastic–plastic stage and (3) falling stage. The linear elastic stage is from initial loading to cracking. The cracking load of HSSWR-reinforced ECC specimens is 23%–31% of the corresponding peak load, while the cracking load of ECC is 56%–62% of the corresponding peak load. This is attributed to the fact that adding HSSWRs in ECC significantly enhanced the tensile strength. In this stage, both ECC and HSSWRs are in the elastic state, and the stress increased linearly as the strain grew. The elastic–plastic stage is from the cracking to the peak load. In this stage, the tensile stress increased nonlinearly with an increase in the tensile strain. The small fluctuations of the curve in this stage were caused by initiation and development of the cracks of HSSWR-reinforced ECC specimens. The HSSWRs and ECC can still carry the load together in the elastic–plastic stage due to the bridging role of PVA fibers after cracking and good bond performance between HSSWRs and ECC. Since the first HSSWR ruptured at the peak load, a falling stage can be observed after peak point in the stress–strain curve.

### 3.3 Cracking Stress and Strain

#### 3.3.1 Effect of HSSWRs Reinforcement Ratio on Cracking Stress and Strain

It can be seen from Table 4 that the cracking strains of HSSWR-reinforced ECC specimens are between 0.0172% and 0.0202%, which are close to those of the

**Table 4** Test results of HSSWR-reinforced ECC specimens.

Group number	$f_{se,cr}$ (MPa)	$\epsilon_{se,cr}$ (%)	$f_{se,u}$ (MPa)	$\epsilon_{se,u}$ (%)	$f_{ws}$ (MPa)	$\epsilon_{ws}$ (%)	$w_{max,ws}$ (mm)	$w_{max,u}$ (mm)	$E_{se}$ (MPa)	$TI_p$	$TI_t$
A1	2.20	0.0190	7.06	3.087	6.52	1.987	0.28	1.13	11,579	0.1670	0.1846
A2	2.25	0.0192	7.74	3.106	6.94	2.215	0.22	1.07	11,719	0.1875	0.2054
A3	2.41	0.0196	8.57	3.158	7.77	1.896	0.20	0.87	12,296	0.2075	0.2235
A4	2.56	0.0202	10.15	3.289	9.55	2.081	0.13	0.73	12,673	0.2462	0.2556
A5	2.44	0.0197	8.65	3.112	7.79	1.908	0.21	0.88	12,386	0.1893	0.2182
B1	1.97	0.0172	6.41	3.293	5.40	1.868	0.12	0.67	11,453	0.1636	0.1894
B2	1.99	0.0173	7.56	3.418	6.71	2.143	0.11	0.60	11,503	0.1811	0.2199
B3	2.07	0.0174	8.42	3.412	7.53	2.295	0.09	0.57	11,897	0.2037	0.2297
B4	2.19	0.0178	9.44	3.335	9.10	2.134	0.08	0.50	12,303	0.2045	0.2675

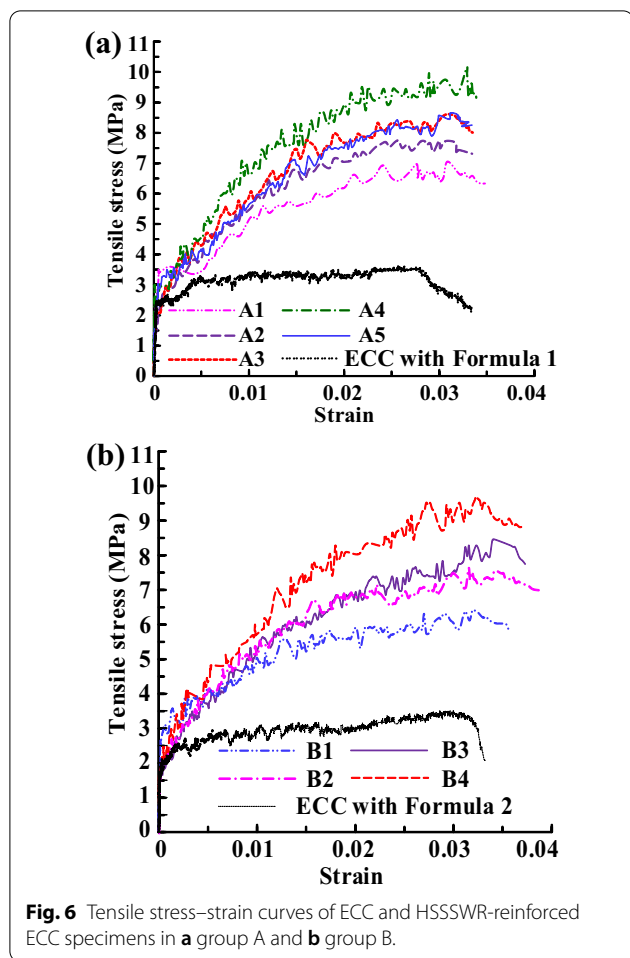


**Fig. 6** Tensile stress–strain curves of ECC and HSSWR-reinforced ECC specimens in **a** group A and **b** group B.

corresponding ECC shown in Table 3, which indicates that adding HSSWRs in ECC hardly had effect on the cracking strain. Fig. 7 shows the comparison of test results of specimens with different reinforcement ratios of longitudinal HSSWRs ( $\rho_w$ ). As shown in Fig. 7, the cracking stress ( $f_{se,cr}$ ) increased slightly with an increase in the reinforcement ratio of HSSWRs ( $\rho_w$ ). Specifically, as indicated in Table 4, the cracking stresses ( $f_{se,cr}$ ) of specimens A1 A2, A3 and A4 increased by 1.4%, 2.7%, 10.0% and 16.9% compared with that of ECC of formula 1, respectively, and the cracking stresses of specimens B1 B2, B3 and B4 increased by 2.6%, 3.6%, 7.8% and 14.1% compared with that of ECC of formula 2, respectively. Moreover, the elastic modulus before cracking ( $E_{se}$ ) of specimens increased with an increase in the reinforcement ratio of HSSWRs ( $\rho_w$ ). These results show that adding HSSWRs in ECC can enhance the cracking stresses and elastic modulus of ECC. This is to be expected, because before cracking, the applied load was carried together by ECC and the internal HSSWRs which were both in elastic stage.

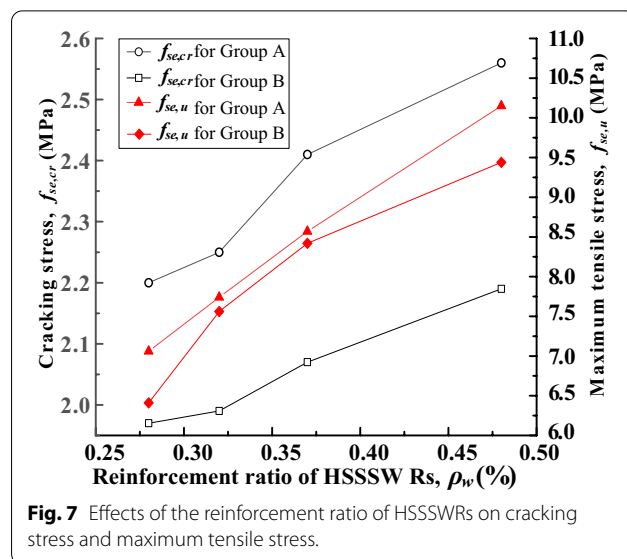


**Fig. 7** Effects of the reinforcement ratio of HSSWRs on cracking stress and maximum tensile stress.

### 3.3.2 Effect of ECC Formula on Cracking Stress and Strain

As shown in Table 4, under the condition of the same reinforcement ratio ( $\rho_w$ ), the cracking stresses of specimens B1, B2, B3 and B4 decreased by 10.5%, 11.6%, 14.1% and 14.5%, compared with that of the corresponding specimen in group A, respectively, and the elastic modulus before cracking ( $E_{se}$ ) of the specimen in group B was lower than that of the corresponding specimen of group A. The reason may be that the cracking stress and elastic modulus of ECC of formula 1 are relatively high compared with those of ECC of formula 2.

### 3.4 Tensile Strength and Its Corresponding Strain

#### 3.4.1 Effect of HSSWRs Reinforcement Ratio on Tensile Strength and Its Corresponding Strain

It can be seen from Fig. 7 and Table 4 that the maximum tensile stresses ( $f_{se,u}$ ) of specimens A1 A2, A3 and A4 increased by 100.0%, 119.3%, 142.8% and 187.5%, respectively, compared with that of ECC of formula 1, and the maximum tensile stresses ( $f_{se,u}$ ) of specimens B1 B2, B3 and B4 increased by 85.3%, 118.5% 143.4% and 172.8%, respectively, compared with that of ECC of formula 2. This indicates that the tensile strength (maximum tensile stress) of HSSWR-reinforced ECC increased significantly with an increase in the reinforcement ratio of HSSWRs. The same phenomenon that the tensile strength would be increased by increasing reinforcement ratio was also observed in steel bars reinforced ECC (Kunieda et al., 2010) and CFRP grid-reinforced ECC (Zhu et al., 2018). This is to be expected, because the applied peak load was carried by ECC and the internal reinforcing materials together. As shown in Table 4, the

strains corresponding to the maximum tensile stresses ( $\epsilon_{se,u}$ ) of the specimens ranged from 3.087% to 3.418%, which were close to the maximum tensile strain of HSSSWR, and were larger than those of the corresponding ECC shown in Table 3. This indicates the deformation capacity of ECC can be effectively improved by adding HSSSWRs in ECC. The reason for enhancing deformation capacity may be that adding HSSSWRs can delay the development of cracks, which contributes to increasing ultimate deformation.

### 3.4.2 Effect of ECC Formula on Tensile Strength and Its Corresponding Strain

The maximum stresses of specimens B1, B2, B3 and B4 decreased by 9.2%, 2.3%, 1.8% and 7.0%, compared with that of the corresponding specimen with the same value of  $\rho_w$  in group A, respectively, which is attributed to the fact that the tensile strength of ECC of formula 2 is relatively low compared with that of ECC of formula 1. The strains corresponding to the maximum stresses of specimens in group B were larger than those of specimens in group A. This demonstrates that adding thickener can improve the deformation capacity of HSSSWR-reinforced ECC by enhancing uniform distribution of PVA fibers.

## 3.5 Tensile Toughness

### 3.5.1 The Method Used to Evaluate Tensile Toughness

Toughness is an important property for evaluating the energy absorption capacity of a composite material before failure, which can be quantitatively described by the integration of the load–displacement curve of the composite material (Dong et al., 2019). In this paper, the tensile toughness of HSSSWR-reinforced ECC (in MJ/m<sup>3</sup>) was calculated by the integration of the stress–strain curve. The total integral area of the stress–strain curve of the HSSSWR-reinforced ECC specimens was defined as the total tensile toughness ( $TI_t$ ), and the integral area of stress–strain curve under peak stress was defined as the peak tensile toughness ( $TI_p$ ). With this method, the total tensile toughness ( $TI_t$ ) and the peak tensile toughness ( $TI_p$ ) for each specimen are calculated and listed in Table 4. The peak tensile toughness and total tensile toughness of ECC with formula 1 calculated using the same method are 0.0890 MJ/m<sup>3</sup> and 0.1043 MJ/m<sup>3</sup>, respectively, and the peak tensile toughness index and total tensile toughness index of ECC with formula 2 are 0.0884 MJ/m<sup>3</sup> and 0.1044 MJ/m<sup>3</sup>, respectively.

### 3.5.2 Effect of HSSSWRs Reinforcement Ratio on Tensile Toughness

The relationship between tensile toughness and reinforcement ratio of longitudinal HSSSWRs is shown in

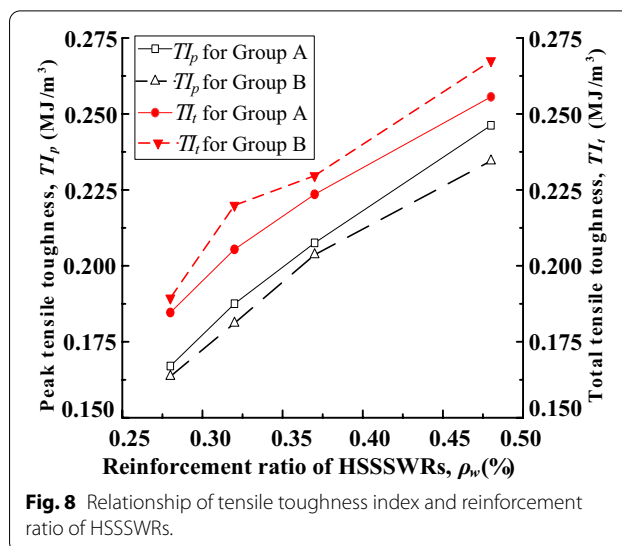


Fig. 8 Relationship of tensile toughness index and reinforcement ratio of HSSSWRs.

Fig. 8. As shown in Fig. 8, the peak tensile toughness and total tensile toughness of HSSSWR-reinforced ECC specimens increased with an increase in the reinforcement ratio of HSSSWRs, and are much higher than those of ECC. This shows that increasing the reinforcement ratio of longitudinal HSSSWRs can effectively improve the energy absorption capacity of the specimens through delaying the development of cracks and enhancement of bearing capacity.

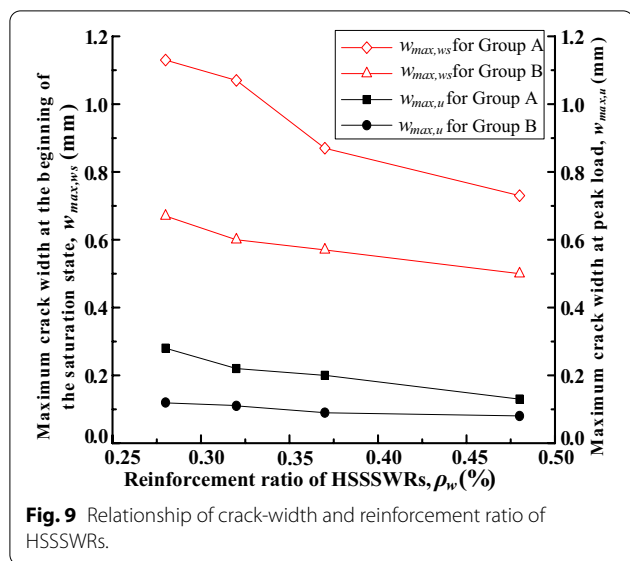
### 3.5.3 Effect of ECC Formula on Tensile Toughness

As indicated in Fig. 8, under the condition of the same reinforcement ratio ( $\rho_w$ ), the peak tensile toughness of the specimen of group A was higher than that of the specimen of group B, but the total tensile toughness of group A was lower than that of group B. The reason may be that adding thickener would reduce the cracking stress and the maximum tensile stress of HSSSWR-reinforced ECC caused by bringing small bubbles in the matrix of formula 2, which makes the peak tensile toughness of group B less than that of group A. However, adding thickener also can enhance uniform distribution of PVA fibers, which can improve the crack-width control and deformation capacity of this composite material, so the total tensile toughness of group B was higher than that of group A.

## 3.6 Analysis of Crack Width

### 3.6.1 Effect of HSSSWRs Reinforcement Ratio on Crack Width

As indicated in Table 4 and Fig. 9, the maximum crack-width at the beginning of the saturation state ( $w_{max,ws}$ ) or at peak load ( $w_{max,u}$ ) decreased with an increase in the reinforcement ratio longitudinal HSSSWRs ( $\rho_w$ ). This demonstrates that increasing the reinforcement ratio contributes to improving crack-width control capacity



of HSSWR-reinforced ECC. The reason may be that the longitudinal HSSWRs can delay the development of cracks through the good bond performance between HSSWRs and ECC.

### 3.6.2 Effect of ECC Formula on Crack Width

It can be seen from Fig. 9 that under the condition of the same reinforcement ratio ( $\rho_w$ ), the maximum crack-width at the beginning of the saturation state ( $w_{max,ws}$ ) or at peak load ( $w_{max,u}$ ) for the specimen with ECC matrix of formula 2 is smaller than that of the specimen with ECC matrix of formula 1. In addition, it can be observed in the test that the specimen with ECC matrix of formula 2 had more cracks and smaller crack spacing compared with the specimen with ECC matrix of formula 1. The above phenomena demonstrate that adding thickener can improve the crack-width control capacity of HSSWR-reinforced ECC due to enhancing uniform distribution of PVA fibers.

### 3.7 Effect of Specimen Width on Tensile Properties

A comparison between test results of specimens A3 and A5 (which are of the same test parameters except for specimen widths) in Fig. 6a and Table 4 shows that the tensile stress–strain curve and the test values of material performance indicators (including  $f_{se,cr}$ ,  $\epsilon_{se,cr}$ ,  $f_{se,u}$ ,  $\epsilon_{se,u}$ ,  $f_{ws}$ ,  $\epsilon_{ws}$ ,  $w_{max,ws}$ ,  $w_{max,u}$ ,  $E_{se}$ ,  $TI_p$  and  $TI_t$ ) for these two specimens are close. This demonstrates that changing specimen width has little effect on the tensile properties of HSSWR-reinforced ECC. This may be because the size effect on tensile properties of ECC can be negligible due to ductile nature of ECC material (Lepech & Li, 2003; Rokugo et al., 2007).

### 3.8 Comparison with ECC Reinforced with Steel Bars or FRP Grids

In order to compare the strengthening effect of HSSWR on ECC with that of other reinforcing materials on ECC, a comparison was made with the previous studies on ECC reinforced with steel bars or FRP grids (Kunieda et al., 2010; Zhu et al., 2018). The comparison of test results of maximum tensile stress ( $f_{se,u}$ ) and its corresponding strain ( $\epsilon_{se,u}$ ) of HSSWR-reinforced ECC specimens in this paper are compared with those of steel bar-reinforced ECC specimens in literature (Kunieda et al., 2010) and CFRP grid-reinforced ECC specimens in literature (Zhu et al., 2018), as shown in Table 5. The comparison presented in Table 5 (S-1-1 versus A1, S-2-1 versus A4, MC1 versus A2, and MC2 versus A4) indicated that the tensile strength ( $f_{se,u}$ ) and its corresponding strain ( $\epsilon_{se,u}$ ) of HSSWR-reinforced ECC specimens are higher, compared with those of steel bar-reinforced ECC specimens or CFRP grid-reinforced ECC specimens, even though both the tensile strength of ECC matrix ( $f_{e,u}$ ) and reinforcement ratio ( $\rho_w$ ) of the steel bar-reinforced ECC specimens or CFRP grid-reinforced ECC specimens are higher than those of HSSWR-reinforced ECC specimens. This demonstrates that HSSWR exhibits better reinforcement efficiency when used to reinforce ECC, compared with steel bars or CFRP grids. This is attributed to the fact that the low tensile strength and early yielding of ordinary steel bars lead to the relatively low tensile strength of ECC reinforced by ordinary steel bars. In addition, the rupture strain of CFRP grids was much lower than the ultimate strain of ECC, which would cause the underutilization of tensile strength and deformation capacity of ECC, so the tensile strength and ultimate strain of CFRP grids-reinforced ECC were relatively low.

## 4 Tensile Stress–Strain Model of HSSWR-Reinforced ECC

### 4.1 Proposed Stress–Strain Model

As analyzed above, the tensile stress–strain curves of HSSWR-reinforced ECC can be divided into three stages. Only the first two stages (elastic stage and elastic–plastic stage) are discussed below considering that the third stage (falling stage) would not be used in practice. So a two-stage model is proposed for describing stress–strain relationship of HSSWR-reinforced ECC in tension, as shown in Eq. (1) and Fig. 10. Fig. 10 shows a typical tensile stress–strain model curve for HSSWR-reinforced ECC. In this model, a linear stress–strain relationship is adopted in the elastic stage, and in the elastic–plastic stage, the total stress is shared by ECC and HSSWR together. In addition, the strength utilization

**Table 5** Comparison of HSSWR-reinforced ECC with ECC reinforced with CFRP grids or steel bars.

Group number	Literature	Reinforcing materials	Specimens in literature (Kunieda et al., 2010) and (Zhu et al., 2018)					HSSWR-reinforced ECC specimens				
			$f_{e,u}$ (N/mm <sup>2</sup> )	$\rho_w$ (%)	$\epsilon_{se,u}$ (%)	$f_{se,u}$ (N/mm <sup>2</sup> )	Group number	$f_{e,u}$ (N/mm <sup>2</sup> )	$\rho_w$ (%)	$\epsilon_{se,u}$ (%)	$f_{se,u}$ (N/mm <sup>2</sup> )	
S-1-1	Kunieda et al., (2010)	Steel bars	5.00	0.3	2.377	6.4	A1	3.53	0.28	3.087	6.52	
S-2-1		Steel bars	5.00	0.6	2.276	7.4	A4	3.53	0.48	3.289	10.15	
MC1	Zhu et al., (2018)	CFRP grids	4.55	0.352	0.81	6.55	A2	3.53	0.32	3.106	7.74	
MC2		CFRP grids	4.55	0.704	0.85	9.99	A4	3.53	0.48	3.289	10.15	

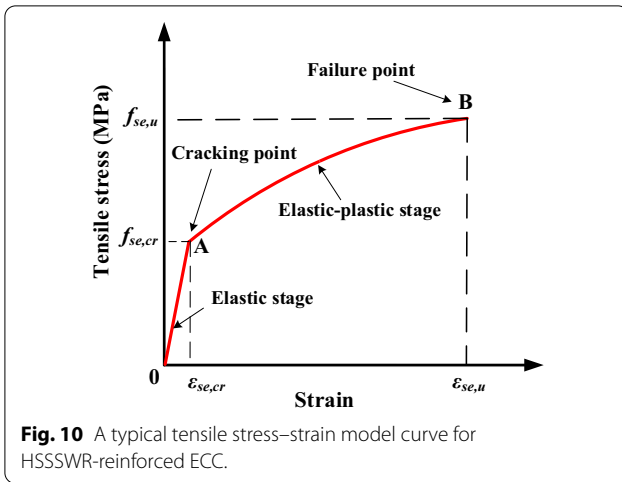


**Fig. 10** A typical tensile stress–strain model curve for HSSSWR-reinforced ECC.

coefficient of HSSSWR ( $\gamma$ ) is introduced in the elastic–plastic stage, considering the inadequate utilization of tensile strength of HSSSWR. This may be caused by the small differences between tensile stresses of longitudinal HSSSWRs in the reinforced ECC under axial tension because of the different tightness of HSSSWRs which may occur during construction. The other reason may be that the relative slip between HSSSWRs and ECC would cause stress hysteresis of longitudinal HSSSWRs:

$$f_{se} = \begin{cases} E_{se}\epsilon_{se} & \epsilon_{se} \leq \epsilon_{se,cr} \\ \gamma f_s \rho_w + f_e & \epsilon_{se,cr} \leq \epsilon_{se} \leq \epsilon_{se,u} \end{cases} \quad (1)$$

where  $f_{se}$  and  $\epsilon_{se}$  are the tensile stress of HSSSWR reinforced ECC and the strain corresponding to  $f_{se}$ , respectively;  $f_s$  and  $f_e$  are the tensile stresses of ECC and longitudinal HSSSWRs, respectively.

## 4.2 Analysis of Model Parameters

### 4.2.1 Elastic Stage

Before the cracking of HSSSWR-reinforced ECC, the external load is carried by HSSSWR and ECC together, which are in the elastic stage. The slip between the HSSSWR and ECC was very small in this stage, which can be ignored (Zhu et al., 2020). According to the strain coordination between HSSSWR and ECC, the force equilibrium equation of HSSSWR reinforced ECC in tension can be expressed by Eq. (2a):

$$E_{se}\epsilon_{se}A_{se} = E_e\epsilon_eA_e + E_s\epsilon_sA_s, \quad (2a)$$

where  $\epsilon_{se}$ ,  $\epsilon_e$  and  $\epsilon_s$  are the tensile strain of HSSSWR reinforced ECC, ECC and HSSSWR, respectively;  $A_{se}$ ,  $A_e$  and  $A_s$  are cross-sectional areas of HSSSWR reinforced ECC, ECC and longitudinal HSSSWRs, respectively. The cross-sectional areas of HSSSWR reinforced ECC and ECC can be assumed to be equal considering the small reinforcement ration of longitudinal HSSSWRs. The strains

of HSSSWR reinforced ECC, ECC and HSSSWR can be considered to be the same according to the strain coordination between HSSSWR and ECC in the elastic stage. Thus, the elastic modulus of HSSSWR-reinforced ECC ( $E_{se}$ ) can be obtained as follows:

$$E_{se} = E_e + E_s \frac{A_s}{A_{se}}. \quad (2b)$$

### 4.2.2 Elastic–Plastic Stage

In the elastic–plastic stage, the stress–strain relationship involved with the stress–strain relationships of both HSSSWRs and ECC. A function form of cubic polynomial is adopted to describe the tensile stress–strain relationship of the HSSSWR based on the regression analyses of the tensile test results of HSSSWRs. The proposed tensile stress–strain model of HSSSWRs is expressed as follows:

$$\frac{f_s}{f_{s,u}} = a \frac{\epsilon_s}{\epsilon_{s,u}} + (3 - 2a) \left( \frac{\epsilon_s}{\epsilon_{s,u}} \right)^2 + (a - 2) \left( \frac{\epsilon_s}{\epsilon_{s,u}} \right)^3, \quad (3)$$

where  $f_{s,u}$  is the ultimate tensile stress of the HSSSWR;  $\epsilon_s$  and  $\epsilon_{s,u}$  are tensile strain and ultimate tensile strain of the HSSSWR, respectively;  $a$  is the material coefficient, which was determined to be 3.33 by regression analyses of test results.

The stress–strain model for ECC in tension proposed in our previous research (Liu, 2018) was adopted to express the tensile stress of ECC ( $f_e$ ):

$$f_e = \begin{cases} \frac{f_{e,cr}}{\epsilon_{e,cr}} \epsilon_e & \epsilon_e \leq \epsilon_{e,cr} \\ \left( 0.31 \frac{\epsilon_e}{\epsilon_{e,u}} + 0.69 \right) f_{e,u} & \epsilon_{e,cr} \leq \epsilon_e \leq \epsilon_{e,u} \end{cases} \quad (4)$$

where  $\epsilon_e$  is the strain corresponding to  $f_e$ . As discussed above, the cracking strain of HSSSWR-reinforced ECC are close to those of ECC due to the strain coordination of these two materials, so  $\epsilon_{se,cr}$  can be set to be equal to  $\epsilon_{e,cr}$ .

### 4.2.3 Strength Utilization Coefficient of HSSSWR

By substituting Eq. (2), Eq. (3) and Eq. (4) into Eq. (1), the tensile constitutive model of HSSSWR-reinforced ECC can be expressed as:

$$f_{se} = \begin{cases} \left( E_e + E_s \frac{A_s}{A_{se}} \right) \epsilon_{se} & \epsilon_{se} \leq \epsilon_{se,cr} \\ \gamma \left[ 3.33 \frac{\epsilon_{se}}{\epsilon_{se,u}} - 3.66 \left( \frac{\epsilon_{se}}{\epsilon_{se,u}} \right)^2 + 1.33 \left( \frac{\epsilon_{se}}{\epsilon_{se,u}} \right)^3 \right] f_{s,u} \frac{A_s}{A_{se}} \\ + \left( 0.31 \frac{\epsilon_{se}}{\epsilon_{se,u}} + 0.69 \right) f_{e,u} & \epsilon_{se,cr} \leq \epsilon_{se} \leq \epsilon_{se,u} \end{cases} \quad (5)$$

The failure mode of HSSSWR-reinforced ECC is the rupture of the longitudinal HSSSWR, so the ultimate strain of HSSSWR reinforced ECC mainly depends on the ultimate strain of HSSSWR, which can be expressed by  $\varepsilon_{se,u} = \varepsilon_{s,u}$ . By regression analysis of test results of all specimens except for specimens A4, A5 and B4 using Eq. (5), the value of strength utilization coefficient of HSSSWR ( $\gamma$ ) and the corresponding coefficient of determination (the square of correlation coefficient) for each specimen was obtained, as shown in Table 6. The values of  $\gamma$  for the specimens in Table 6 are very close to each other, so the value of  $\gamma$  in Eq. (5) was taken to be the average value (0.73).

According to the proposed constitutive model expressed by Eq. (5) and theory of mechanical equilibrium, the following equations for calculating the cracking stress ( $f_{se,cr}$ ) and maximum tensile stress ( $f_{se,u}$ ) of HSSSWR reinforced ECC can be obtained as follows:

$$\begin{cases} f_{se,cr} = \left( E_e + E_s \frac{A_s}{A_{se}} \right) \varepsilon_{se,cr} \\ f_{se,u} = 0.73 f_{s,u} \frac{A_s}{A_{se}} + f_{e,u} \end{cases} \quad (6)$$

#### 4.3 Model Verification

In order to verify the accuracy of the proposed tensile constitutive model of HSSSWR reinforced ECC, Fig. 11 presents the comparison of the test stress–strain curves from initial loading to peak load of all specimens in Table 1 and the proposed model expressed by Eq. (5). The peak point of the stress–strain curve (the end of the stress–strain curve) in Fig. 11 indicates the first HSSSWR rupture point. As shown in Fig. 11, the proposed model agrees well with the test stress–strain curves in the elastic stage. In the elastic–plastic stage, the proposed model consists with the overall trends of the test stress–strain curves, considering the fluctuations of the test curves due to the appearance and development of cracks in this stage. The comparison indicates that the proposed model can be applied to describe the stress–strain relationship of HSSSWR reinforced ECC. Besides, the test values of cracking

stress and maximum tensile stress (tensile strength) are compared with the calculated values using Eq. (6), as shown in Table 7. In Table 7,  $t$  and  $c$  represent test values and calculated values, respectively, and  $r$  is the ratio of the test value to the calculated value. In Table 7, the average value of the ratios of test values to calculated values for cracking stresses of specimens is 1.02 with a variation coefficient of 0.03. In addition, the average value of the ratios of test values to calculated values for tensile strengths of specimens is 1.08 with a variation coefficient of 0.05. This indicates that Eq. (6) can be accepted to predict the cracking stress and tensile strength of HSSSWR-reinforced ECC.

## 5 Conclusions

The tensile performance of HSSSWR-reinforced ECC is investigated experimentally and theoretically. The effects of influence factors (reinforcement ratio of HSSSWR, formula of ECC and width of the test specimen) on tensile characteristics of HSSSWR-reinforced ECC were discussed and revealed. A stress–strain model is developed for HSSSWR reinforced ECC in tension:

1. Adding HSSSWRs in ECC was verified to be an effective measure to enhance both the tensile strength and deformation capacity of ECC under tension. Compared with steel bars or CFRP grids, HSSSWR exhibits better reinforcement efficiency when used to reinforce ECC. The final failure of HSSSWR-reinforced ECC was characterized by longitudinal HSSSWR rupture and pullout of PVA fibers at the main cracked section. Multiple cracks, good crack-width control capacity and high deformation capacity of HSSSWR reinforced ECC were observed due to the bridging role of the internal PVA fibers and retarding effect of HSSSWRs on the development of cracks.
2. Increasing the reinforcement ratio of longitudinal HSSSWRs is suggested to be used to improve the tensile strength, crack-width control capacity, deformation capacity and tensile toughness of HSSSWR reinforced ECC under tension. The enhancement effect of increasing the reinforcement ratio of HSSSWR on the cracking stress of HSSSWR reinforced ECC is much lower than that on the tensile strength. The tensile properties of the HSSSWR reinforced ECC plates are almost not affected by increasing the plate width.
3. Adding thickener in ECC can be adopted to significantly improve the crack-width control capacity and deformation capacity of HSSSWR reinforced ECC under tension due to enhancing uniform distribution of PVA fibers, although the cracking stresses and tensile strength of HSSSWR reinforced ECC would be

**Table 6** Fitting values of  $\gamma$  for specimens.

Group number	$\gamma$	$R^2$
A1	0.73	0.9267
A2	0.72	0.9459
A3	0.75	0.9607
B1	0.71	0.9157
B2	0.72	0.9755
B3	0.72	0.9325

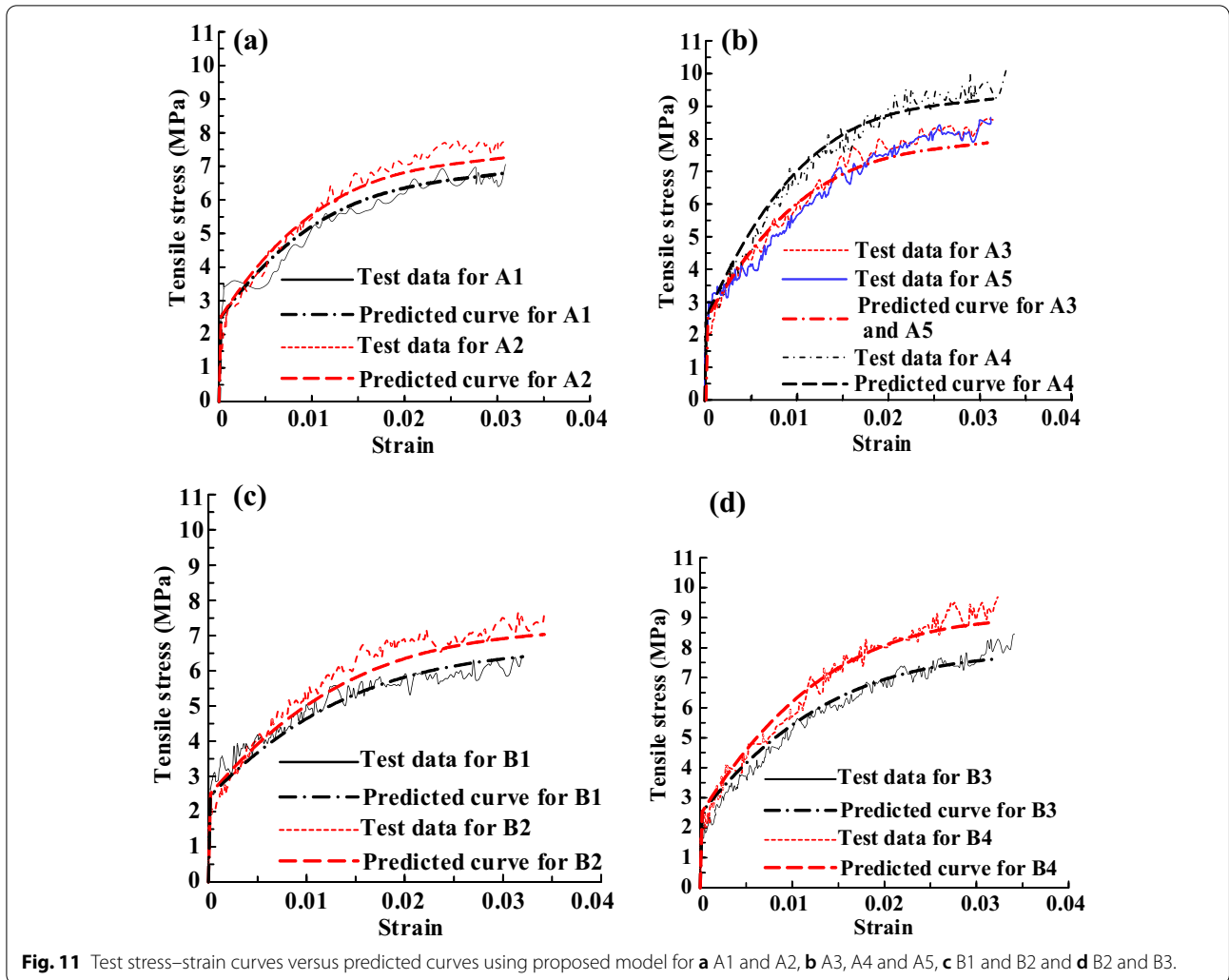


**Fig. 11** Test stress–strain curves versus predicted curves using proposed model for **a** A1 and A2, **b** A3, A4 and A5, **c** B1 and B2 and **d** B2 and B3.

**Table 7** Comparison of calculated results of cracking stress and tensile strength by using Eq. (6) and test results.

Group number	$f_{se,cr}$ (MPa)			$f_{se,u}$ (MPa)		
	<i>t</i>	<i>c</i>	<i>r</i>	<i>t</i>	<i>c</i>	<i>r</i>
A1	2.20	2.24	0.98	7.06	6.74	1.05
A2	2.25	2.27	0.99	7.74	7.20	1.07
A3	2.41	2.33	1.03	8.57	7.82	1.10
A4	2.56	2.42	1.06	10.15	8.67	1.17
A5	2.44	2.35	1.04	8.65	7.82	1.11
B1	1.97	1.99	0.99	6.41	6.67	0.96
B2	1.99	2.01	0.99	7.56	7.13	1.06
B3	2.07	2.03	1.02	8.42	7.75	1.09
B4	2.19	2.09	1.05	9.44	8.60	1.10

slightly decreased as a result of bringing small bubbles in the matrix. The cracking strain of HSSWR reinforced ECC is close to that of the ECC matrix.

4. The tensile stress–strain curve of HSSWR reinforced ECC can be divided into three stages, including linear elastic stage, elastic–plastic stage and fall-

ing stage. The proposed tensile stress–strain model and calculation equations of model parameters were validated to be acceptable for predicting tensile mechanics of HSSWR reinforced ECC through being compared with the test results.

#### Acknowledgements

This work was financially supported by the National Natural Science Foundations of China (Grant Numbers 51879243, U1804137); National Key Research and Development Project (Grant Number 2017YFC1501204); China Postdoctoral Science Foundation (2020M672236); and Ministry of housing and urban rural development science and technology program (No. 2019-K-059).

#### Authors' contributions

Xinling Wang: conceptualization, methodology, writing—original draft, funding acquisition. Guanghua Yang: investigation, data curation, writing—original draft. Wenwen Qian: investigation, data curation, writing—original draft. Ke Li: supervision, writing—review and editing, funding acquisition, project administration. Juntao Zhu: supervision, funding acquisition, project administration. All authors read and approved the final manuscript.

#### Authors' information

Xinling Wang is a Full Professor in School of Civil Engineering at Zhengzhou University, Zhengzhou, Henan, China.  
Guanghua Yang is a graduate student in School of Civil Engineering at Zhengzhou University, Zhengzhou, Henan, China.  
Wenwen Qian is an employee of JZFC architectural design Co. Ltd. at Zhengzhou, Henan, China  
Ke Li and Juntao Zhu are Associate Professors in School of Civil Engineering at Zhengzhou University, Zhengzhou, Henan, China.

#### Funding

National Natural Science Foundations of China, Grant Numbers: 51879243 and U1804137; National Key Research and Development Project, Grant Number: 2017YFC1501204. China Postdoctoral Science Foundation, Grant Number: 2020M672236. Ministry of housing and urban rural development science and technology program, Grant Number: No. 2019-K-059.

#### Availability of data and materials

The data in this paper will be supplied upon request.

#### Declarations

#### Competing interests

The authors declare that they have no known competing financial interests or personal relationships that could have appeared to influence the work reported in this paper.

#### Author details

<sup>1</sup>School of Civil Engineering, Zhengzhou University, Science Avenue 100#, Zhengzhou 450001, China. <sup>2</sup>JZFC Architectural Design Co. Ltd, Zhengzhou 450001, China.

Received: 26 April 2021 Accepted: 15 October 2021  
Published online: 06 November 2021

#### References

- Al-Gemeel, A. N., Zhuge, Y., & Youssf, O. (2019). Experimental investigation of basalt textile reinforced engineered cementitious composite under apparent hoop tensile loading. *Journal of Building Engineering*, *23*, 270–279. <https://doi.org/10.1016/j.jobbe.2019.01.037>
- ACI Committee 224. Control of cracking in concrete structures. Farmington Hills, MI: American Concrete Institute; 2001.
- Dong, D. F., Zhou, D. C., & Ashour, A. (2019). Flexural toughness and calculation model of super-fine stainless wire reinforced reactive powder concrete. *Cement and Concrete Composites*, *104*, 103367. <https://doi.org/10.1016/j.cemconcomp.2019.103367>
- Esmaeeli, E., Manning, E., & Barros, J. A. O. (2013). Strain hardening fiber reinforced cement composites for the flexural strengthening of masonry elements of ancient structures. *Construction and Building Materials*, *38*, 1010–1021. <https://doi.org/10.1016/j.conbuildmat.2012.09.065>
- Fischer, G., & Li, V. C. (2002a). Effect of matrix ductility on deformation behavior of steel reinforced ECC flexural members under reversed cyclic loading conditions. *ACI Materials Journal*, *99*, 781–790.
- Fischer, G., & Li, V. C. (2002b). Influence of matrix ductility on tension-stiffening behavior of steel reinforced engineered cementitious composites (ECC). *ACI Structural Journal*, *99*(1), 104–114.
- Ghai, R., Bansal, P. P., & Kumar, M. (2018). Strengthening of RCC beams in shear by using SBR polymer-modified ferrocement jacketing technique. *Advances in Civil Engineering*, *2018*, 4028186. <https://doi.org/10.1155/2018/4028186>
- Guan, Y., Yuan, H., & Ge, Z. (2018). Flexural properties of ECC-concrete composite beam. *Advances in Civil Engineering*, *2018*, 3138759. <https://doi.org/10.1155/2018/3138759>
- Hossain, K. M. A. (2018). Bond strength of GFRP bars embedded in engineered cementitious composite using RILEM beam testing. *International Journal of Concrete Structures and Materials*, *12*(1), 6. <https://doi.org/10.1186/s40069-018-0240-0>
- Hu, B., Zhou, Y., & Xing, F. (2019). Experimental and theoretical investigation on the hybrid CFRP-ECC flexural strengthening of RC beams with corroded longitudinal reinforcement. *Engineering Structures*, *200*, 109717. <https://doi.org/10.1016/j.engstruct.2019.109717>
- Huang, H., Liu, B. Q., & Wu, T. (2011). Analysis of stiffness and cracks of shear strengthened beam with stainless steel wire mesh and PPM China. *Civil Engineering Journal*, *44*, 32–38. <https://doi.org/10.3724/SPJ.1077.2011.00271>
- Hung, C. C., & Chen, Y. S. (2016). Innovative ECC jacketing for retrofitting shear-deficient RC members. *Construction and Building Materials*, *111*, 408–418. <https://doi.org/10.1016/j.conbuildmat.2016.02.077>
- Kim, S. H., & Kim, D. K. (2011). Seismic retrofit of rectangular RC bridge columns using wire mesh wrap casing. *KSCCE Journal of Civil Engineering*, *15*(7), 1227–1236. <https://doi.org/10.1007/s12205-011-0881-x>
- Kunieda, M., Hussein, M., & Ueda, N. (2010). Enhancement of crack distribution of UHP-SHCC under axial tension using steel reinforcement. *Journal of Advanced Concrete Technology*, *8*(1), 49–57. <https://doi.org/10.3151/jact.8.49>
- Lepech, M., & Li, V. C. (2003). Preliminary findings on size effect in ECC structural members in flexure. *Brittle Matrix Composites*, *7*, 57–66. <https://doi.org/10.1533/9780857093103.57>
- Li, B. B., & Xiong, H. B. (2019). Tensile behavior of basalt textile grid reinforced Engineering Cementitious Composites Part B-Engineering. *Composites Part B-Engineering*, *156*, 185–200. <https://doi.org/10.1016/j.compositesb.2018.08.059>
- Li, V. C. (2019). High-performance and multifunctional cement-based composite material. *Engineering*, *5*(2), 250–260. <https://doi.org/10.1016/j.eng.2018.11.031>
- Li, V. C., Horikoshi, T., & Ogawa, A. (2004). Micromechanics-based durability study of polyvinyl alcohol-engineered cementitious composite. *ACI Materials Journal*, *101*(3), 242–248. <https://doi.org/10.1016/j.vacuum.2004.02.004>
- Li, V. C., & Leung, C. K. Y. (1992). Steady-state and multiple cracking of short random fiber composite. *Journal of Engineering Mechanics*, *118*(11), 2246–2264. [https://doi.org/10.1061/\(ASCE\)0733-9399\(1992\)118:11\(2246\)](https://doi.org/10.1061/(ASCE)0733-9399(1992)118:11(2246))
- Li, V. C., Mishra, D. K., & Wu, H. C. (1995). Matrix design for pseudo strain-hardening fiber reinforced cementitious composites. *Materials and Structures*, *28*(10), 586–595. <https://doi.org/10.1007/BF02473191>
- Li, V. C., Stang, H., & Krenchel, H. (1993). Micromechanics of crack bridging in fibre-reinforced concrete. *Materials & Structures*, *26*, 486–494. <https://doi.org/10.1007/BF02472808>
- Li, X., Xie, H., & Yan, M. (2018). Eccentric compressive behavior of reinforced concrete columns strengthened using steel mesh reinforced resin concrete. *Applied Sciences-Basel*, *8*(10), 1827. <https://doi.org/10.3390/app8101827>
- Liu, W.K. (2018). Study on the compression and tensile properties and the constitutive model of ECC. Zhengzhou university. (in Chinese).

- Ministry of Housing and Urban-Rural Development of the People's Republic of China (MOHURD): Code for Design of Concrete Structures (GB50010–2010), Beijing, 2015 (in Chinese).
- Naaman, A. E., & Reinhardt, H. W. (2006). Proposed classification of HPRC composites based on their tensile response. *Materials and Structures*, 39(5), 547–555. <https://doi.org/10.1617/s11527-006-9103-2>
- Pan, Y., Wu, C., Cheng, X., & Li, V. C. (2020). Impact fatigue behaviour of GFRP mesh reinforced engineered cementitious composites for runway pavement. *Construction and Building Materials*, 230, 116898. <https://doi.org/10.1016/j.conbuildmat.2019.116898>
- Qeshta, I. M. I., Shafiqh, P., & Jumaat, M. Z. (2015). Flexural behaviour of RC beams strengthened with wire mesh-epoxy composite. *Construction and Building Materials*, 79, 104–114. <https://doi.org/10.1016/j.conbuildmat.2015.01.013>
- Qeshta, I. M. I., Shafiqh, P., & Jumaat, M. Z. (2016). Research progress on the flexural behaviour of externally bonded RC beams. *Archives of Civil and Mechanical Engineering*, 16(4), 982–1003. <https://doi.org/10.1016/j.acme.2016.07.002>
- Qi, B., Kong, Q., & Qian, H. (2018). Study of impact damage in PVA-ECC beam under low-velocity impact loading using piezoceramic transducers and PVDF thin-film transducers. *Sensors*, 18(3), 671. <https://doi.org/10.3390/s18020671>
- Raouf, S. M., Koutas, L. N., & Bournas, D. A. (2017). Textile-reinforced mortar (TRM) versus fibre-reinforced polymers (FRP) in flexural strengthening of RC beams. *Construction and Building Materials*, 151, 279–291. <https://doi.org/10.1016/j.conbuildmat.2017.05.023>
- Rokugo, K., Uchida, Y., & Moriyama, M. (2007). Direct tensile behavior and size effect of strain-hardening fiber-reinforced cement-based composites (SHCC). In: Proceedings of the 6th International Conference on Fracture Mechanics of Concrete and Concrete Structures, Catania, Italy, Jun 17–22, 1429–1434.
- Shang, X., Yu, J., & Li, L. (2019). Strengthening of RC structures by using engineered cementitious composites: A review. *Sustainability*, 11(12), 1–18. <https://doi.org/10.3390/su11123384>
- Shermi, C., & Dubey, R. N. (2017). Study on out-of-plane behaviour of unreinforced masonry strengthened with welded wire mesh and mortar. *Construction and Building Materials*, 143, 104–120. <https://doi.org/10.1016/j.conbuildmat.2017.03.002>
- Wang, X. L., Zhao, Y. K., & Zhou, Q. W. (2020). Study on bond-slip property of high strength stainless steel strand and ECC. *Journal of Huazhong University of Science and Technology. Nature Science*, 48, 108–113. <https://doi.org/10.13245/j.hust.201219> (in Chinese).
- Yuan, F., Chen, M. C., & Pan, J. L. (2020). Flexural strengthening of reinforced concrete beams with high-strength steel wire and engineered cementitious composites. *Construction and Building Materials*, 254, 119284. <https://doi.org/10.1016/j.conbuildmat.2020.119284>
- Yuan, F., Pan, J. L., & Wu, Y. F. (2014). Numerical study on flexural behaviors of steel reinforced engineered cementitious composite (ECC) and ECC/concrete composite beams. *Science China-Technological Sciences*, 57(003), 637–645. <https://doi.org/10.1007/s11431-014-5478-4>
- Zheng, Y. Z., Wang, W. W., & Brigham, J. C. (2016). Flexural behaviour of reinforced concrete beams strengthened with a composite reinforcement layer: BFRP grid and ECC. *Construction and Building Materials*, 115, 424–437. <https://doi.org/10.1016/j.conbuildmat.2016.04.038>
- Zhou, J. J., Pan, J. L., & Leung, C. K. Y. (2015). Mechanical behavior of fiber-reinforced engineered cementitious composites in uniaxial compression. *Journal of Materials in Civil Engineering*, 27(1), 04014111. [https://doi.org/10.1061/\(ASCE\)MT.1943-5533.0001034](https://doi.org/10.1061/(ASCE)MT.1943-5533.0001034)
- Zhu, J. T., Zhang, K., & Wang, X. L. (2020). Bond-slip relational model between high-strength stainless steel wire mesh and ECC. *China Civil Engineering Journal*, 53, 83–92. <https://doi.org/10.15951/j.tmgcxb.2020.04.008> (in Chinese).
- Zhu, Z. F., Wang, W. W., & Harries, K. A. (2018). Uniaxial tensile stress-strain behavior of carbon-fiber grid-reinforced engineered cementitious composites. *Journal of Composites for Construction*, 22, 6. [https://doi.org/10.1061/\(ASCE\)CC.1943-5614.0000891](https://doi.org/10.1061/(ASCE)CC.1943-5614.0000891)

## Publisher's Note

Springer Nature remains neutral with regard to jurisdictional claims in published maps and institutional affiliations.

Submit your manuscript to a SpringerOpen® journal and benefit from:

- Convenient online submission
- Rigorous peer review
- Open access: articles freely available online
- High visibility within the field
- Retaining the copyright to your article

Submit your next manuscript at ► [springeropen.com](https://www.springeropen.com)